STM JOURNALS

Journal of
Polymer & Composites

ISSN: 2321-2810 (Online)
ISSN: 2321-8525 (Print)
Volume 13, Special Issue 6, 2025
DOI (Journal): 10.37591/JoPC

https://journals.stmjournals.com/jopc

Research JoPC

Energy Storage Properties of hy-BST3/PVDF Nanocomposite for Dielectric Capacitor Application

Ankit Dwivedi[1,*]

Abstract

In the present research work, we have synthesized the ferroelectric ceramic $Ba_{0.7}$ $Sr_{0.3}TiO_3$ (BST3)/PVDF (Polyvinylidene difluoride). Polymer nanocomposites for energy storage applications, designed to synergistically combine the high dielectric permittivity of hydroxylated barium strontium titanate (hy-BST3) with the mechanical flexibility and electroactive properties of poly(vinylidene fluoride) (PVDF). Hydroxylated Barium Strontium Titanate (hy-BST3) has been synthesized using the sol-gel combustion method followed by surface hydroxylation using H_2O_2 to achieve nanoscale particles with improved uniformity and reduced agglomeration. BST3/PVDF nanocomposites have been synthesized using the solution casting method with 90 wt. % PVDF polymers as a matrix and 10 wt.% BST3 ceramic as nano,fillers and their dielectric and energy storage properties have been investigated. The solution casting method is a technique used to synthesize nanocomposites in film form. The influence of hy-BST3 and BST3 content on the dielectric constant, dielectric loss and energy storage properties were systematically evaluated. The results reveal that the incorporation of hy-BST3 significantly enhances the dielectric constant of PVDF while maintaining relatively low dielectric loss. XRD analysis has been performed to check the successful synthesis of nanocomposites. We have obtained improved dielectric and ferroelectric properties in the case of hy-BST3/PVDF nanocomposite, which makes it better for energy storage applications requiring high energy density, reliability and mechanical flexibility.

Keywords: Ferroelectric, Nanocomposites, Solution casting method, PVDF, BST3, Energy storage density.

INTRODUCTION

The accelerating demand for compact, efficient and high-performance energy storage systems has intensified research in dielectric capacitors, particularly for pulsed power and embedded electronic applications [1-6]. In the evolving landscape of energy storage technologies, dielectric capacitors offer rapid charge–discharge rates (<1 μs), high power density, thermal stability and exceptional reliability, making them indispensable for pulsed-power systems, electric vehicles and flexible electronics [7-10]. However, traditional polymer-based dielectric materials often suffer from limited energy storage density, mainly due to their relatively low dielectric constant, despite their high breakdown strength and processability. Among various polymer dielectrics, Poly(vinylidene fluoride) (PVDF), a semi-crystalline ferroelectric polymer, is extensively explored for energy storage because of its high dielectric breakdown strength, mechanical flexibility, light weight, and processability [10]. Poly(vinylidene fluoride)

***Author for Correspondence**
Ankit Dwivedi

[1]Assistant Professor, Department of Physics, Govt. Model Science (Autonomous) College, Jabalpur, Madhya Pradesh, India

Received Date: July 03, 2025
Accepted Date: August 23, 2025
Published Date: November 25, 2025

Citation: Ankit Dwivedi. Energy Storage Properties of hy-BST3/PVDF Nanocomposite for Dielectric Capacitor Application. Journal of Polymer and Composites. 2025; 13(Special Issue 6): S908–S918p.

(PVDF) and its copolymers (e.g., P(VDF–TrFE), P(VDF–HFP)) are among the most extensively studied ferroelectric polymers for dielectric capacitor applications. PVDF is characterized by its high breakdown strength (~600–700 kV/mm), chemical stability, mechanical flexibility and good processability. Moreover, its intrinsic ferroelectric β-phase exhibits spontaneous polarization, making it highly attractive for dielectric and electroactive applications. Despite these advantages, conventional polymeric dielectrics like poly(vinylidene fluoride) (PVDF) possess relatively low energy storage densities, significantly lower than electrochemical capacitors and batteries. This discrepancy arises from PVDF's lower dielectric permittivity (~10 at 1 kHz) and discharge efficiency [11].

To overcome this limitation, various strategies have been proposed, with particular emphasis on incorporating high-permittivity ceramic fillers into the PVDF matrix to form nanocomposites [12,13]. Among the various classes of dielectric materials, polymer–ceramic nanocomposites have gained attention as promising materials because of their ability to synergistically integrate the beneficial properties of both polymers and ceramics. Incorporating these ceramics into the PVDF matrix allows for a synergistic effect: the ceramic nanoparticles increase the dielectric constant through interfacial and dipolar polarization mechanisms, while PVDF ensures high breakdown strength and mechanical flexibility [14-16]. Ceramic fillers like barium titanate (BT) and barium–strontium titanate (BST) exhibit high dielectric constants and strong field-dependent polarization, which can enhance the effective dielectric properties of the composite meanwhile it suffer from low breakdown strength and poor processability in bulk form [8-11]. Recent developments in nanotechnology and surface engineering have enabled the synthesis of nanoscale ceramic fillers with controlled size, morphology and surface chemistry. Nanoparticles are preferred over micro-sized fillers due to their larger specific surface area, which increases interfacial interaction and polarization, but they must be uniformly dispersed to avoid agglomeration and local field distortion that can lower breakdown strength [14]. The use of nanoparticles or nanowires with appropriate surface functionalization can significantly improve filler dispersion, reduce dielectric loss and enhance the interfacial interaction between the polymer matrix and ceramic inclusions. For instance, hydroxylation, silanization, or the use of surfactants can tailor the ceramic surface to bond effectively with the fluoropolymer chains, leading to a more uniform microstructure and improved energy storage characteristics [17-19]. Energy storage density is directly proportional to dielectric constant and the square of the breakdown strength of the dielectric material. It is evident that achieving superior energy storage performance requires both a high dielectric constant and a high breakdown strength.

BST/PVDF nanocomposites thus present an effective hybrid solution—combining BST's high permittivity with PVDF's mechanical flexibility and dielectric robustness. However, achieving high energy density while preserving breakdown strength is non-trivial due to interface weaknesses and filler dispersion challenges. Barium strontium titanate ($Ba_{1-x}Sr_xTiO_3$, BST), a lead-free ferroelectric ceramic, has emerged as a promising material because of its tunable dielectric properties, high permittivity and low dielectric loss near room temperature. The dielectric constant of BST is strongly composition-dependent; particularly, compositions near the morphotropic phase boundary (MPB), such as BST3 ($Ba_{0.7}Sr_{0.3}TiO_3$), exhibit enhanced dielectric response and field-induced polarization characteristics suitable for energy storage applications [20-22]. When embedded into a PVDF matrix, BST nanoparticles can induce interfacial polarization and increase the local electric field distribution, thereby enhancing the overall dielectric and energy storage behavior of the composite. $Ba_{0.7}Sr_{0.3}TiO_3$ (BST3) having ferroelectric behaviour and tunable dielectric properties have attracted the attention of researchers.

In this work, we focus on the synthesis and detailed energy storage evaluation of surface hydroxylated BST3/PVDF nanocomposite films fabricated via the solution casting method. The influence of hydroxylation of BST3 filler on the dielectric properties, polarization behavior and energy storage density is systematically investigated. This study aims to provide insights into the structure–property relationships governing the dielectric performance of BST-based polymer nanocomposites for next-generation capacitor applications.

MATERIALS AND SYNTHESIS METHODS

Barium Strontium Titanate (BST3) ceramic powders were synthesized using a sol-gel assisted combustion method [23]. The precursor materials included stoichiometric quantities of Barium Nitrate ($Ba(NO_3)_2$, LOBA Chemie, 99% purity), Strontium Carbonate ($SrCO_3$, Sigma Aldrich, 98% purity) and Titanium Isopropoxide ($C_{12}H_{28}O_4Ti$, Sigma Aldrich, >97% purity), which served as the sources for Ba^{2+}, Sr^{2+} and Ti^{4+} ions, respectively. Citric acid monohydrate ($C_6H_8O_7 \cdot H_2O$, Qualikems, >97% purity) was used as the organic fuel to facilitate combustion. Distilled water and high-purity ethanol (C_2H_5OH, 99.9% by volume) acted as solvents, while aqueous ammonia solution (25% NH_3, GSC) was employed to adjust the pH of the sol.

Initially, strontium carbonate was dissolved in diluted nitric acid to produce strontium nitrate. Subsequently, stoichiometric amounts of barium nitrate, the prepared strontium nitrate solution, and citric acid were each dissolved in 50 mL of distilled water in separate beakers. These solutions were combined and continuously stirred at 120 °C using a magnetic stirrer to ensure homogenization. Titanium isopropoxide was pre-stabilized by adding it dropwise into ethanol under constant stirring to prevent premature hydrolysis. This stabilized TTIP-ethanol solution was then gradually introduced into the mixed precursor solution. Following this, ammonia solution was carefully added to adjust the pH to approximately 7, promoting gel formation.

The resulting mixture was stirred continuously at 120 °C for 24 hours, allowing the sol to transition into a gel. The obtained gel was oven-dried at 150 °C to remove residual solvents and moisture. The resulting dry mass was finely ground into powder and subsequently calcined at 750 °C to achieve phase-pure BST3 ceramic powder.

The BST3/PVDF nanocomposite films were synthesized via a conventional solution casting technique. Initially, 90 wt.% of poly(vinylidene fluoride) (PVDF) and 10 wt.% of BST3 ceramic nanoparticles were individually dispersed in N,N-dimethylformamide (DMF) using ultrasonic agitation to ensure complete dissolution and deagglomeration [19]. The resulting solutions were subsequently combined and subjected to continuous magnetic stirring for 12 hours to facilitate uniform dispersion of the BST3 nanoparticles within the polymer matrix. The homogeneous slurry was then cast into a clean Petri dish and dried in a hot-air oven at 120 °C for 12 hours to yield a flexible composite film. For comparison purposes, a pristine PVDF film was also synthesized following the same procedure, without the inclusion of any ceramic fillers.

To improve nanoparticle dispersion and interfacial compatibility within the polymer matrix, surface hydroxylation of BST3 was carried out. Specifically, 10 wt.% of BST3 powder was treated with 20 mL of hydrogen peroxide (H_2O_2) and refluxed at 106 °C for 6 hours. The hydroxylated particles were subsequently dried at 120 °C for 10 hours. Successful surface modification was verified via Fourier-transform infrared (FTIR) spectroscopy, which confirmed the presence of hydroxyl functional groups on the BST3 surface.

The modified BST3 powder was then dispersed in DMF and the solution casting process described earlier was repeated to fabricate the hydroxylated BST3/PVDF (hy-BST3/PVDF) nanocomposite film. Consequently, three distinct film types were prepared: pure PVDF, BST3/PVDF, and hy-BST3/PVDF nanocomposites, all employing the same base methodology to ensure consistency in structural and property comparisons.

RESULTS AND DISCUSSION

The XRD patterns of the BST3/PVDF nanocomposites were recorded over a 2θ range of 10–60° using a Rigaku Smartlab benchtop X-ray diffractometer to confirm the formation of the composites. Additionally, TGA-DSC analysis was conducted to evaluate their thermal stability. FTIR analysis has been performed for hy-BST3 powder to check the successful hydroxylation of BST3 powder. FTIR

spectroscopy was also performed for nanocomposite films. FESEM analysis was also performed to study the microstructure of the nanocomposite film. The surfaces of each nanocomposite were electroded using air-dried silver paste for the measurements of dielectric properties and the measurements were performed in the temperature range 30°C to 120°C. For PE hysteresis loop measurement, both surfaces of the films are electroded with air dried silver paste and measurement was performed at room temperature and 50 Hz frequency via varying electric field.

X-ray Diffraction Analysis

X-ray diffraction (XRD) analysis was done to investigate the crystalline nature of the PVDF film, BST3/PVDF film and hydroxylated BST3/PVDF film. The XRD pattern of the pure PVDF film exhibited prominent peaks at 2θ values of 18.60°, 20.60°, 26.60°, and 36.10°, which are characteristic of the predominant α-phase of PVDF, consistent with previous literature [24]. These results confirm the semicrystalline nature of the PVDF film. In the nanocomposite films, diffraction peaks corresponding to both the BST3 powder and the PVDF film were observed, confirming the successful formation of the composite films. XRD pattern of BST3/PVDF film have dominant α phase while XRD pattern of hy-BST3/PVDF film have dominant β phase which is shown in Fig. 1. These peaks are consistent with previously reported literature. The presence of the peaks corresponding to the BST3 powder indicates a cubic structure with Pm3m space group (JCPDS ref code: 34-0411) [9,23]. Thus, the BST3 crystals are present in the composite film and are integrated with the PVDF film, forming a single and cohesive material.

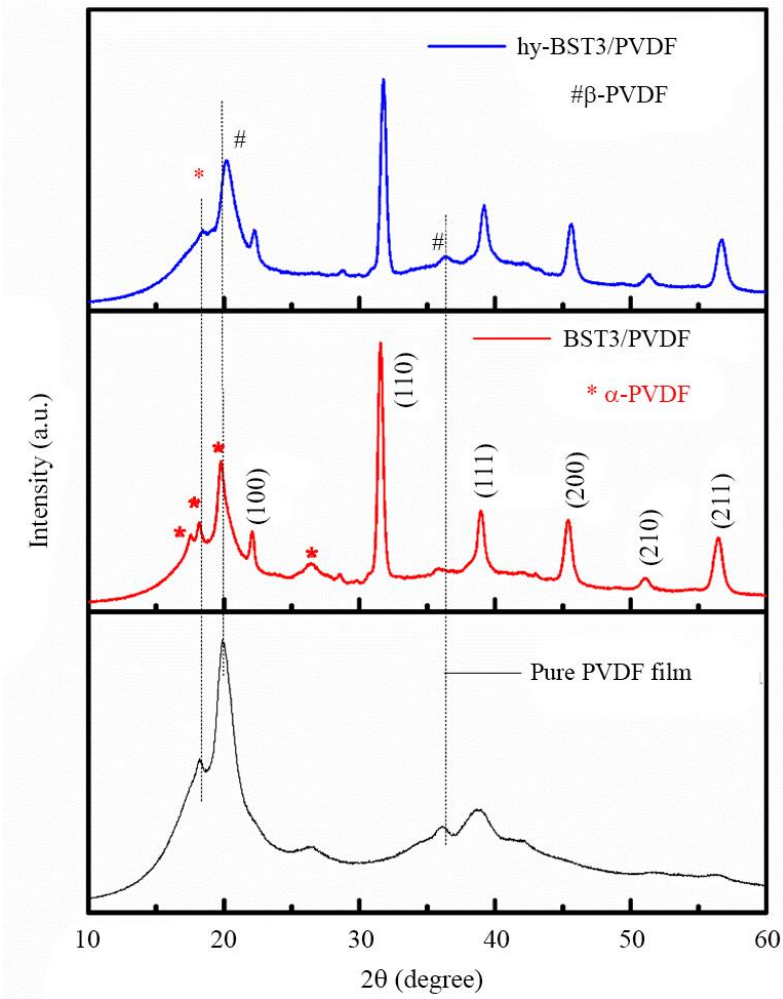

Figure 1. XRD plot for pure PVDF Film, BST3/PVDF composite and hy-BST3/PVDF composite film.

FTIR Analysis

FTIR analysis has been performed for BST3 powder, hy-BST3 Powder, BST3/PVDF and hy-BST3/PVDF composite film and spectra is shown in Figure 2. FTIR spectra of hy-BST3 powder have been recorded to ensure the hydroxylation of BST3 powder. In FTIR spectra of hy-BST3 powder, there is a peak at 1386 cm^{-1} which corresponds to -OH group as reported in available literature and is absent in the FTIR spectra of BST3 powder [25]. Thus, confirmation of hydroxylation of BST3 powder happens. In the FTIR spectra of BST3/PVDF and hy-BST3/PVDF composite film, it is observed that there is dominance of electroactive phases (β and γ) in comparison to the nonpolar α phase, which is a good sign for the composites. Transmittance peaks in the nanocomposites corresponding to wave number 1071 cm^{-1}, 1170 cm^{-1}, 506 cm^{-1} named as β, peaks corresponding to 476 cm^{-1}, 832 cm^{-1}, 876 cm^{-1}, 1231 cm^{-1} named as γ and peaks corresponding to 1401 cm^{-1} are named as α phase of PVDF polymer [26,27]. These observed peaks are in good agreement with previously reported literature.

FESEM Analysis

FESEM image has been recorded for the surface of pure PVDF film, BST3/PVDF and hy-BST3/PVDF nanocomposite film and is shown in Figure 3. Due to the semi-crystalline nature of PVDF, we observe spherulitic domains or phase-separated crystalline and amorphous regions in the FESEM image of pure PVDF film which is shown in Figure 3(a). The FESEM image of the BST3/PVDF composite film shows dispersed ceramic nanoparticles embedded within the PVDF matrix, which is shown in Figure 3(b). Poor interfacial adhesion might be evident from gaps or voids around some ceramic particles, which can act as weak points during electrical breakdown or mechanical stress. The FESEM image of the hy-BST3/PVDF composite film reveals better dispersion and distribution of nanoparticles compared to unmodified BST3, which is shown in Figure 3(c). Hydroxylation improves surface compatibility between ceramic fillers and the PVDF polymer, resulting in intimate contact at the interface, reduced voids, smooth surface and improved film density. The morphology is typically more uniform indicating enhanced interaction due to hydroxyl groups forming hydrogen bonds or interfacial interactions with the PVDF chains.

The FESEM-EDX spectra in Figure 4 represent the presence of Barium, Strontium, Titanium, Oxygen, Carbon and Fluorine. The elements Ba, Sr, Ti, O, C and F originate from the PVDF-based composite structure because of the presence of BST3. Each element in the composites has a

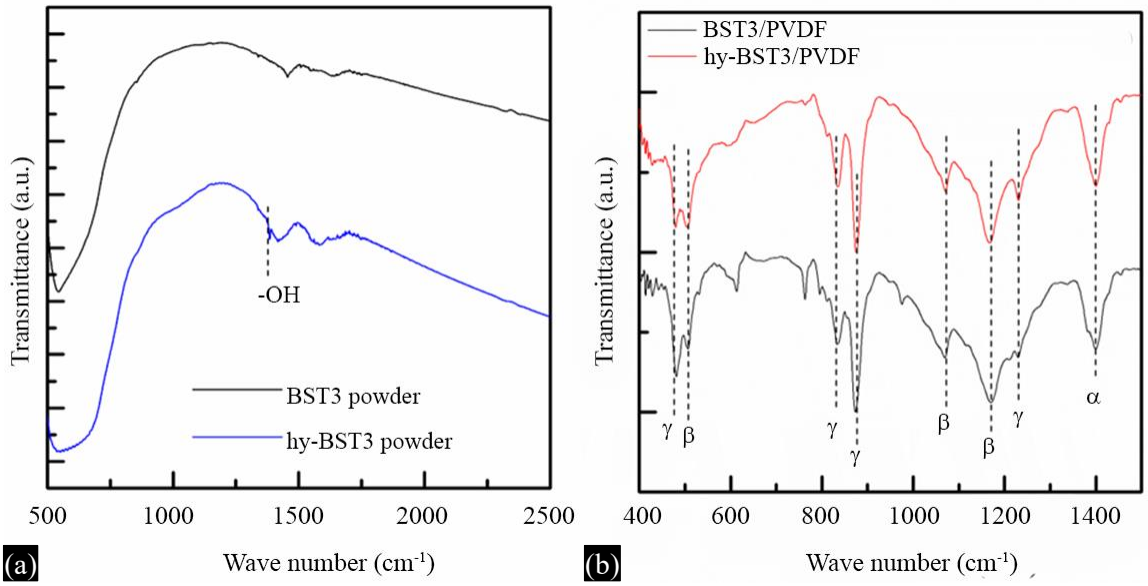

Figure 2. FTIR spectra of (a) BST3 and hy-BST3 Powder, (b) BST3/PVDF and hy-BST3/PVDF composite film

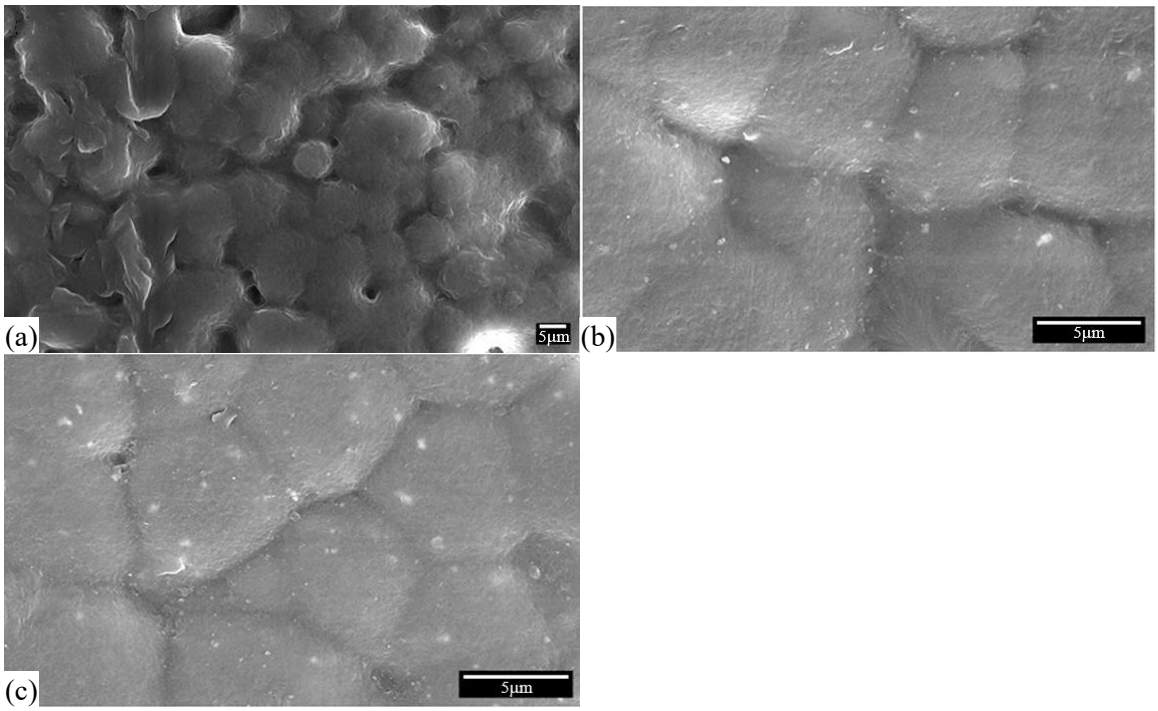

Figure 3. FESEM image of (a) pure PVDF film, (b) BST3/PVDF composite, (c) hy-BST3/PVDF composite film

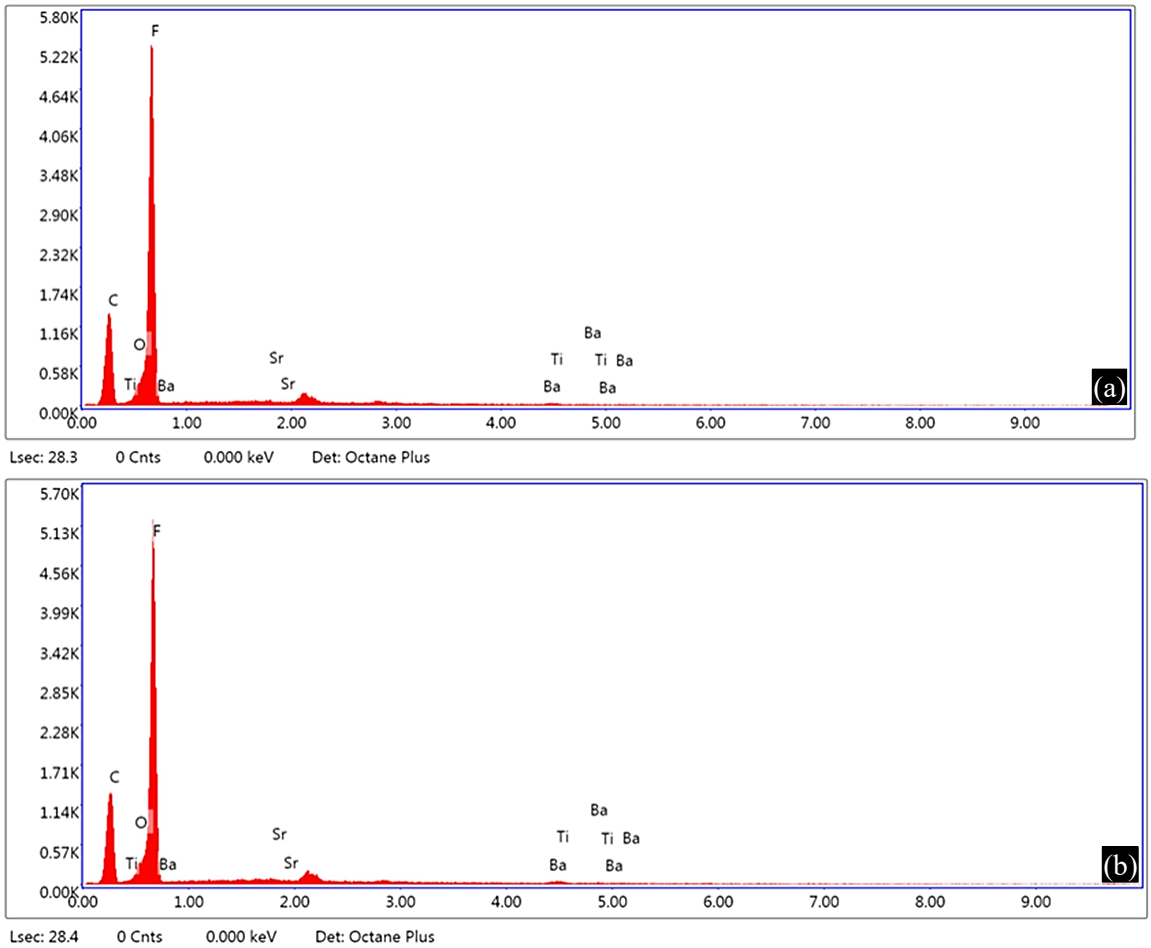

Figure 4. FESEM- EDX spectra of (a) BST3/PVDF composite, (b) hy-BST3/PVDF composite film

characteristic peak, and its peak height represents the percentage concentration of each element in PVDF matrix [28]. These results show the successful synthesis of BST3 based PVDF polymer composites.

Thermal analysis using TGA/DSC

Thermogravimetric analysis (TGA) was carried out to evaluate the thermal stability of the composite film. As shown in Figure 5(a), no significant weight loss was detected up to 450 °C, indicating good thermal stability within this range. Beyond 450 °C, however, a sharp decrease in weight was observed, suggesting mass loss in the composite. This is likely due to an endothermic process involving the dissociation of the ceramic filler from the polymer matrix and the pyrolysis of the PVDF polymer. These results are consistent with previously reported data [19]. Differential scanning calorimetry (DSC) analysis was performed to determine the nature of energy release or absorption. DSC plot shows the endothermic peak at 168 ^{0}C in the composites as well as in PVDF film which is shown in Figure 5(b). As, area under the curve in DSC plot shows the degree of crystallinity. Thus, from the DSC curve, it can be concluded that the degree of crystallinity has been increased in the case of composites in comparison to pure PVDF film. The highest degree of crystallinity has been obtained in case of hy-BST3/PVDF nanocomposite film because the area under the curve of DSC plot is highest in the case of hy-BST3/PVDF composite film.

Dielectric Properties

Figure 6 illustrates the temperature-dependent dielectric constant and loss tangent (tan δ) of the PVDF film, BST3/PVDF and hy-BST3/PVDF nanocomposites within the temperature range of 30–120 °C at 1 kHz frequency. The dielectric permittivity of pure PVDF, BST3/PVDF and hy-BST3/PVDF films exhibit an increasing trend with rising temperature. For pure PVDF, a significant increase in permittivity occurs beyond 80 °C due to the enhanced molecular mobility of PVDF chains at higher temperatures. In contrast, the presence of BST3 fillers in the nanocomposites restricts molecular motion, resulting in improved temperature stability. Furthermore, a reduction in the loss tangent is observed for the nanocomposites at elevated temperatures, indicating superior thermal stability compared to the pure PVDF film. The dielectric permittivity value has been increased in the case of hy-BST3/PVDF nanocomposites in comparison to BST3/PVDF composites and the dielectric permittivity value has been increased in the case of BST3/PVDF composites in comparison to pure PVDF film. Thus, in the case of hy-BST3/PVDF composites, we have obtained the enhanced and highest value of dielectric permittivity having least dielectric loss. Thus hy-BST3/PVDF nanocomposite

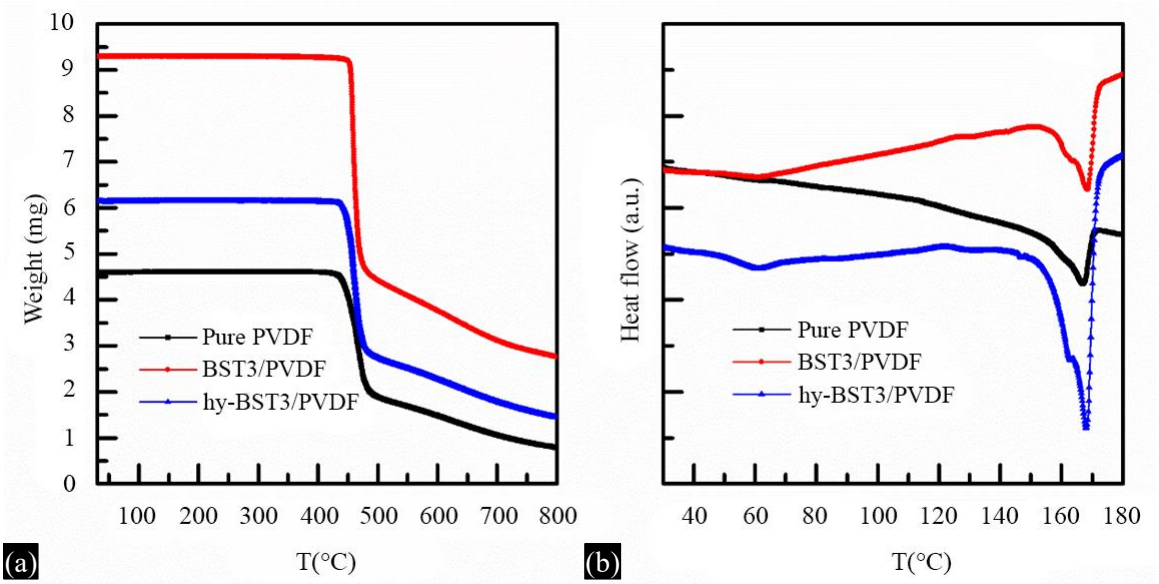

Figure 5. (a) TGA plot for pure PVDF, BST3/PVDF composite and hy-BST3/PVDF composite film, (b) DSC plot for PVDF, BST3/PVDF composite and hy-BST3/PVDF composite film.

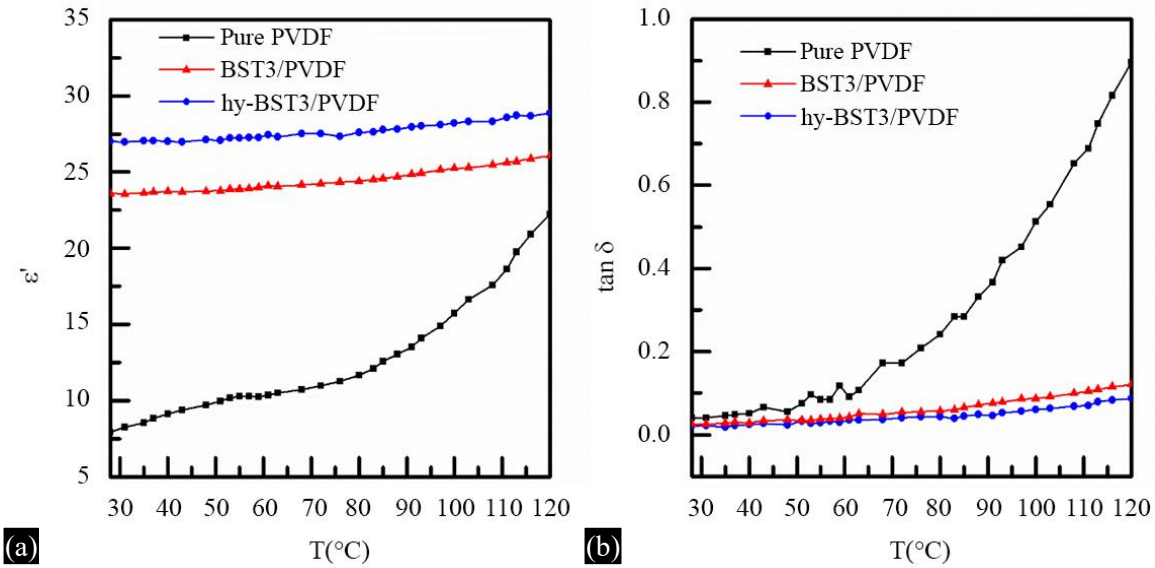

Figure 6. Variation of dielectric permittivity and dielectric loss vs. temperature for PVDF Film, BST3/PVDF composite and hy-BST3/PVDF composite film at 1 KHz frequency.

film shows better dielectric properties. The enhancement in the dielectric properties of hydroxylated BST/PVDF nanocomposite films can be primarily attributed to Maxwell-Wagner interfacial interactions and microstructural modifications induced by hydroxyl functionalization of the ceramic nanoparticles. Hydroxylation of BST nanoparticles introduces –OH functional groups that enhance the chemical affinity between the ceramic surface and the polar PVDF chains through hydrogen bonding. This chemical interaction reduces interfacial defects such as voids and weak boundary layers, resulting in more effective stress transfer and polarization continuity across the interface. The presence of hydroxyl groups on the surface of BST nanoparticles significantly enhances their compatibility with the polar PVDF matrix through hydrogen bonding and dipole–dipole interactions. Consequently, a more homogeneous microstructure is achieved, contributing to a higher effective dielectric constant. Furthermore, the strong interfacial interactions between hydroxylated BST and PVDF promote the nucleation and stabilization of the β-phase in PVDF, as evidenced by FTIR and XRD analysis. The β-phase, being the polar crystalline form of PVDF, possesses a significantly higher dielectric constant compared to the non-polar α-phase, thereby enhancing the overall dielectric response of the composite. The combination of these effects results in an overall improvement in both the dielectric constant and the energy storage performance of the nanocomposite film[29-31].

P-E hysteresis Loop Analysis

Figure 7 illustrates the P–E hysteresis loops of the pure PVDF film, the BST3/PVDF composite and the hy-BST3/PVDF composite at a frequency of 50 Hz. The pristine PVDF film exhibits very low polarization, which can be attributed to the presence of the non-polar α-phase. Incorporating BST3 nanopowder into the polymer matrix significantly increases the polarization due to Maxwell–Wagner–Sillars (MWS) polarization. While the remanent polarization shows a modest rise, the area under the hysteresis loop (∫EdP), reflecting the energy density increases markedly, suggesting enhanced energy storage capability compared to pure PVDF. In the case of the hy-BST3/PVDF nanocomposite, a further increase in polarization is observed at the same electric field as the BST3/PVDF composite. This substantial improvement is likely due to the presence of the polar β-phase of PVDF. Although the remanent polarization increases only slightly in the hy-BST3/PVDF nanocomposite compared to the other samples, the dramatic enhancement in overall polarization results in a much higher ∫EdP value, thereby boosting the energy density. Additionally, the polarization continues to rise with increasing electric field, with no evidence of saturation even up to 800 kV/cm, indicating the nanocomposite could potentially sustain even higher electric fields.

The observed lack of saturation polarization even at high electric fields (up to 800 kV/cm) indicates that the dominant polarization mechanisms may not solely arise from intrinsic ferroelectric domain alignment. Instead, this behavior can be attributed to a combination of factors including interfacial polarization at the ceramic-polymer boundaries (Maxwell–Wagner–Sillars effect), space charge accumulation facilitated by surface hydroxyl groups and incomplete alignment of dipolar domains within the PVDF matrix. The hydroxyl-functionalized BST nanoparticles introduce localized traps at the interface, promoting charge accumulation which enhances polarization without saturation. Additionally, the structural confinement imposed by the ceramic fillers may hinder full polymer chain alignment, further suppressing saturation[32-34]. It is well known that among the α, β and γ phases of PVDF, the β-phase exhibits the highest polarity due to its all-trans (TTTT) chain conformation, leading to superior dipolar alignment under an electric field. The introduction of hydroxylated BST nanoparticles facilitates strong interfacial interactions with the PVDF matrix, particularly through hydrogen bonding and dipole–dipole interactions. These interactions effectively promote the transformation of the non-polar α-phase into the electroactive β-phase. The increased β-phase content enhances the dielectric constant and contributes to higher breakdown strength due to better phase compatibility and reduced local field concentration. Consequently, the energy storage density of the nanocomposite is significantly improved, highlighting the critical role of phase engineering in optimizing PVDF-based dielectric materials[35,36]. The recoverable energy density and efficiency for pure PVDF film, BST3/PVDF composite and hy-BST3/PVDF composite film has been calculated qualitatively using P-E hysteresis curve at electric field of 792 kV/cm and is shown in Table 1. From Table 1, we see that hy-BST3/PVDF composite film have highest recoverable energy density among all the samples while its efficiency have been reduced in comparision to BST3/PVDF composite film.

Table 1. Comparision of recoverable energy density and efficiency for pure PVDF film, BST3/PVDF composite and hy-BST3/PVDF composite film

Sample	Recoverable energy density Urec (J/cm^3)	Efficiency η (%)
Pure PVDF film	0.28	87
BST3/PVDF composite film	0.35	66
hy-BST3/PVDF composite film	0.37	61

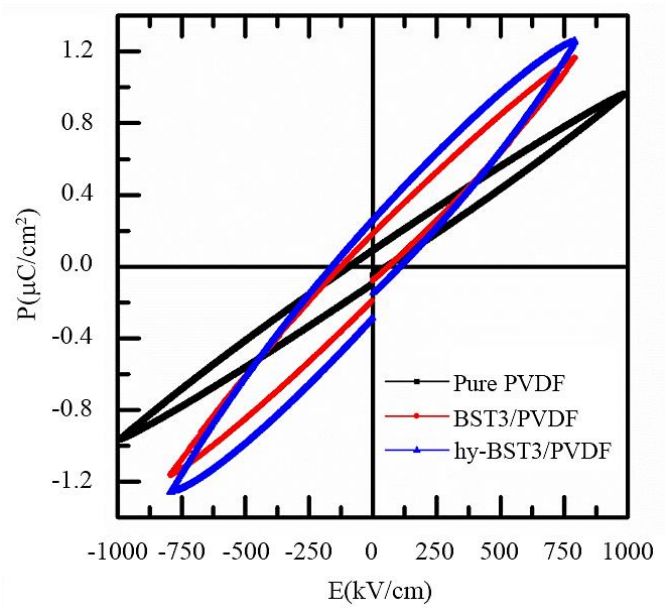

Figure 7. P-E hysteresis curve for PVDF Film, BST3/PVDF composite and hy-BST3/PVDF composite film.

CONCLUSION

XRD pattern confirms that BST3/PVDF nanocomposites were synthesized successfully using solution casting method. The DSC plot shows that the hy-BST3/PVDF composite have highest degree of crystallinity. TGA helps in understanding the thermal stability of the nanocomposite. FTIR spectra of the BST3 powder indicate that there is successful hydroxylation of BST3 powder. The hy-BST3/PVDF nanocomposite has improved dielectric and ferroelectric properties which can be seen from dielectric and P-E hysteresis curves. Thus, hy-BST3/PVDF nanocomposite is a more suitable material for energy storage purposes, as can be seen from the dielectric and P-E hysteresis curve of the nanocomposite. These properties make it well-suited for use in dielectric capacitors.

REFERENCES

1. Hedayati M, Taheri-Nassaj E, Yourdkhani A, et al. Dielectric properties and energy storage behavior of PVDF-based nanocomposites filled with $BaTiO_3$ nanotubes and nanofibers: a comparative study. Ceram Int. 2025
2. Wu H, Zhuo F, Qiao H, et al. Polymer-/ceramic-based dielectric composites for energy storage and conversion. Energy Environ Mater. 2022;5(2):486-514
3. Tan DQ. The search for enhanced dielectric strength of polymer-based dielectrics: a focused review on polymer nanocomposites. J Appl Polym Sci. 2020;137(36):49379.
4. Muduli SP, Lipsa L, Parida S. Current trends of characterization techniques for PVDF and related composite piezoelectric materials for nanogenerator. Discov Polym. 2025;2(1):14.
5. Wang Z, Ye J, Liu S, et al. Enhanced energy storage capability of hydroxylated $BiFeO_3$/PVDF composites designed by compositionally gradient multilayer structures. J Alloys Compd. 2025;1010:177194.
6. Sharma S, Mishra SS, Kumar R, et al. Recent progress on polyvinylidene difluoride-based nanocomposites: applications in energy harvesting and sensing. New J Chem. 2022;46:18613-18646.
7. Zhang X, Shen Y, Yang Y, et al. Giant energy density and improved discharge efficiency of solution-processed polymer nanocomposites for dielectric energy storage. Adv Mater. 2016;28(10):2055–61.
8. Xie LY, Qi H, Zhang H, et al. Core@double-shell structured $BaTiO_3$-polymer nanocomposites with high dielectric constant and low dielectric loss for energy storage application. J Phys Chem C. 2013;117(44):22525–37.
9. Song Y, Chen Q, Chen G, et al. Significant enhancement in energy density of polymer composites induced by dopamine-modified $Ba_{0.6}Sr_{0.4}TiO_3$ nanofibers. Appl Phys Lett. 2012;101(15):152904.
10. Liu SH, Xie LY, Qi H, et al. Significantly enhanced dielectric property in PVDF nanocomposites flexible films through a small loading of surface hydroxylated $Ba_{0.6}Sr_{0.4}TiO_3$ nanotubes. J Mater Chem A. 2014;2(47):18040–6.
11. Yu K, Chen Q, Liu H, et al. Poly(vinylidene fluoride) polymer-based nanocomposites with enhanced energy density by filling with polyacrylate elastomers and $BaTiO_3$ nanoparticles. Appl Phys Lett. 2014;104(8):082904.
12. Li JJ, Hao X, Zhang L, et al. High-field antiferroelectric behaviour and minimized energy loss in poly(vinylidene-co-trifluoroethylene)-graft-poly(ethyl methacrylate) for energy storage application. J Mater Chem. 2012;22(46):23468–76.
13. Huang X, Jiang P. Core-shell structured high-k polymer nanocomposites for energy storage and dielectric applications. Adv Mater. 2015;27(4):546–54.
14. Dang ZM, Yuan JK, Yao SH, et al. Flexible nanodielectric materials with high permittivity for power energy storage. Adv Mater. 2013;25(44):6334–65.
15. Wang Y, Zhou X, Lin M, et al. High-energy density in aromatic polyurea thin films. Appl Phys Lett. 2009;94(20):202905.
16. Li W, Meng Q, Zheng Y, et al. Electric energy storage properties of poly(vinylidene fluoride). Appl Phys Lett. 2010;96(19):192905.
17. Yuan X, Chung TCM. Cross-linking effect on dielectric properties of polypropylene thin films and applications in electric energy storage. Appl Phys Lett. 2011;98(6):062901.

18. Wu S, Li W, Lin M, et al. Aromatic polythiourea dielectrics with ultrahigh breakdown field strength, low dielectric loss, and high electric energy density. Adv Mater. 2013;25(14):1734–40.
19. Gyan DS, Dwivedi A. Structural and electrical characterization of $NaNbO_3$–PVDF nanocomposites fabricated using cold sintering synthesis route. J Appl Phys. 2019;125(2):024104.
20. Hilton AD, Ricketts BW. Dielectric properties of $Ba_{1-x}Sr_xTiO_3$ ceramics. J Phys D Appl Phys. 1996;29(5):1321–6.
21. Ma W, Cross LE. Flexoelectric polarization of barium strontium titanate in the paraelectric state. Appl Phys Lett. 2002;81(19):3440–2.
22. Liou J, Chiou B. Dielectric characteristics of doped $Ba_{1-x}Sr_xTiO_3$ at the paraelectric state. Mater Chem Phys. 1997;51(1):59–63.
23. Shen C, Liu Q. Sol–gel synthesis and spark plasma sintering of $Ba_{0.5}Sr_{0.5}TiO_3$. Mater Lett. 2004;58(17):2302–6.
24. Gregorio R Jr. Determination of the α, β, and γ crystalline phases of poly(vinylidene fluoride) films prepared at different conditions. J Appl Polym Sci. 2006;100(4):3272–9.
25. Sharma N, Kushwaha HS, Sharma SK, et al. Fabrication of $LaFeO_3$ and RGO-$LaFeO_3$ microspheres-based gas sensors for detection of NO_2 and CO. RSC Adv. 2020;10(3):1297–308.
26. Shepelin NA, Glushenkov AM, Lussini VC, et al. New developments in composites, copolymer technologies and processing techniques for flexible fluoropolymer piezoelectric generators for efficient energy harvesting. Energy Environ Sci. 2019;12(4):1143–76.
27. Gregorio R, Ueno EM. Effect of crystalline phase, orientation and temperature on the dielectric properties of poly(vinylidene fluoride) (PVDF). J Mater Sci. 1999;34(18):4489–500.
28. Leonard K, Sathyamurthy S, Paranthaman M. Characterization of $BaZrO_3$ nanoparticles prepared by reverse micelle synthesis. Chem Mater. 2005;17(15):4010–7.
29. Prateek, Bhunia R, Garg A, et al. Probing the interface activation in designing defect-free multilayered polymer nanocomposites for dielectric capacitor applications. J Phys Chem C. 2020;124(42):22914-22924.
30. Hou D, Shen J, Zhou J, et al. PVDF-based nanocomposites with increased crystallinity and polar phases toward high energy storage performance. ACS Appl Energy Mater. 2024;7(21):9974-9985.
31. Zhu N, Zhou J, Zhang L, et al. Design and characterization of molecular, crystal and interfacial structures of PVDF-based dielectric nanocomposites for electric energy storage. Soft Matter. 2023;19:4401-4431
32. Saba S, Mustafa GM, Saleem M, et al. Ferroelectric polymer/ceramic nanocomposites with low energy losses. Polym Compos. 2020;41(8):3271-3281.
33. Yang M, Guo M, Xu E, et al. Polymer nanocomposite dielectrics for capacitive energy storage. Nat Nanotechnol. 2024;19:588-603.
34. Dhabliya D, Husain SO, Hussein AHA, et al. Polymer ceramic-based dielectric composites for energy storage and conversion. E3S Web Conf. 2024;564:11018.
35. Jiang Y, Zhou M, Shen Z, et al . Ferroelectric polymers and their nanocomposites for dielectric energy storage applications. APL Mater. 2021;9(2):020901.
36. Yadav MK, Das T, Shukla A, et al. Enhanced β-phase and ferroelectric properties of the BTO–BHF/PVDF-based flexible nanocomposite film for energy storage device application. ACS Appl Electron Mater. 2025.

